Effects of Tempering Temperature on the Microstructure and Creep Resistance of X22CrMoV12-1 Steel Used on Steam Turbine Blades

Franco Wronski Comeli[1,*], Alexandre da Silva Rocha[2], Carlos Augusto Silva de Oliveira[3], Georges Lemos[3], Richard de Medeiros Castro[4]

[1]Department of Mechanical Maintenance, ENGIE, Capivari de Baixo-SC, Brazil
[2]Department of Metallurgical Engineering, UFRGS - Federal University of Rio Grande do Sul, Porto Alegre-RS, Brazil
[3]Department of Materials Engineering, UFSC - Federal University of Santa Catarina, Florianópolis-SC, Brazil
[4]Department of Mechanical Engineering, SATC College, Criciúma-SC, Brazil

Abstract The development of manufacturing processes and materials for components of steam turbines are very important to increase the reliability and availability of power generation. These materials must have resistance to corrosion and creep, the effects of prolonged exposure to high temperature has a strong influence on metallurgical stability, causing them to fail in operation. Precipitation hardening stainless steels are thermally treated to improve their creep resistance through the formation of precipitates. The purpose of this study is to evaluate the influence of tempering temperature on the microstructure and the creep resistance of X22CrMoV12-1 steel. The microstructure was characterized by optical microscopy (OM), scanning electron microscopy (SEM) and transmission electron microscopy (TEM). Analysis of the tempered samples showed a microstructure composed of martensite with $M_{23}C_6$ carbides located along the martensite slats. Higher tempering temperatures promoted reduction of hardness, yield and ultimate tensile with increased elongation. The X22CrMoV12-1 tempered steel at 690°C showed superior performance of its creep resistance among tempered temperatures tested.

Keywords Creep, X22CrMoV12-1, Tempering, Turbines

1. Introduction

Some materials have a great ability to maintain their mechanical properties at elevated temperatures, good examples include components applied in turbines, space industry and heat exchangers. For these applications, the performance is limited by the operating conditions that may be supported by the materials used. For example, fuel economy and pressure required in modern turbogenerators are strongly dependent and limited by the high temperature resistance of the materials used in their hotter sections [1, 2]. Each material operates at different temperatures, in Fig. 1 is presented the performance of metals and alloys when compared to the tensile stress after 100 hours at elevated temperatures. Note that, among the metals, X22CrMoV12-1 steel shows great resistance the temperature [3].
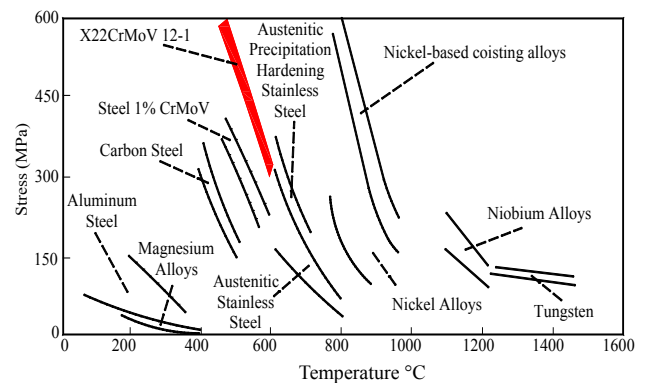
Figure 1. Ratio of stress to rupture after 100 hours with the temperature for various alloys adapted by the authors [3]

The main feature of materials resistant to high temperatures is the ability to support stresses during long periods at operating temperatures near its melting point. For applications at high temperatures, strain based on time (creep) should be considered [4, 5].

Steam turbines for electrical generation operate by tapering and directing the steam in a circumferential flow, creating a vortex whose rate can exceed 400 m/s. Steam is a

dense fluid with high temperature. Its mechanical action on the turbine blades demands it to be made of materials with high resistance to creep. On the blades' design we must consider the action of steam's flow forces, centrifugal forces, differential pressure and high temperature, and its corrosive potential. The vibration forces of the blades should also be considered since it destabilizes the system [6].

Fig. 2 shows the low-pressure rotor that will be installed in 2019 in Unit 5 - UTLB of the Jorge Lacerda Thermoelectric Complex, in which we can see the blades at each stage of pressure.
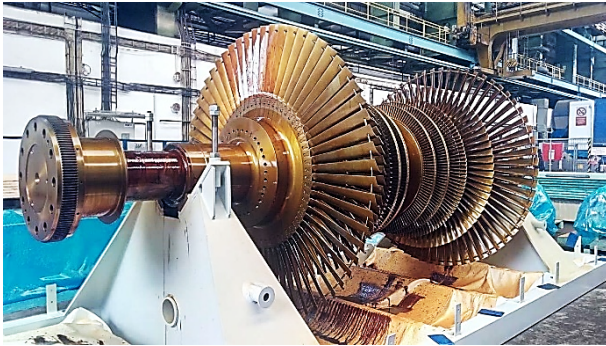

Figure 2.   Low Pressure Rotor Unit 5 UTLB, Brazil

The variety of alloys used in steam turbine components is relatively small, partly because the materials are required to have high thermal properties, such as expansion and conductivity, and partly because these high temperature mechanical properties must have an affordable cost. The selection of these alloys depends on the temperatures and maximum pressures each specific component will be exposed, which in turn depends on the specific design of the turbine [7].

Creep resistant steels used in power plants or in the chemical and petrochemical industry are low carbon, containing carbide forming elements such as: chromium, molybdenum and vanadium. They are used at temperatures between 480 and 565°C and tensions between 15 and 30 MPa for periods of over 30 years [8]. One of the most critical factors determining the integrity of components at high temperatures (greater than 30% of the absolute melt temperature) is their creep behavior, which can cause materials to slowly and continuously deform and eventually fail under constant or intermittent stress [9].

Among the latest developments in precipitation hardened martensitic stainless steels is the X22CrMoV12-1 one developed for high temperature applications such as components of steam turbines whose peak temperatures can reach 600°C [8, 9]. This steel is widely used in thermoelectric power plants all over the world, as it has higher yield strength than ferritic and martensitic steels. Its microstructure makes it able to maintain its mechanical properties during long periods of operation, while the chemical composition ensures resistance to oxidation even in constant contact with high temperature steam [10].

The microstructural variation that occurs in a material under constant stress at high temperatures leads to a deformation that is a function of time, defined as creep, in general can include elastic and plastic deformation [11]. Turbine blades in thermoelectric power plants may have residual life limited by this deformation or even to fracture during operation [12].

The microstructure of the *precipitation hardening stainless steels* X22CrMoV12-1 is a result of the heat treatment initiated by the solubilization of precipitates between 1020 and 1070°C followed by cooling to air, oil or water and, finally, with tempering between 680 and 740°C.

The purpose of this study was to evaluate the influence of tempering temperature on the microstructure and creep resistance of tempered X22CrMoV12-1 steel at 660, 690 and 740°C. To this end, tempered steel at these temperatures was submitted to creep tests at 600°C with constant loads of 160 and 175 MPa.

The purpose of the microstructural characterization was to determine the existing phases and constituents, besides allowing a more detailed knowledge about the influence of the tempering temperature on the microstructure.

2. Experimental Procedure

2.1. Characterization of Steel

The Chemical analysis was performed by optical emission spectrometry on a SPECTRO CAST equipment, the result was calculated from the average of five analyses.

To determine the α '/ γ transition, precipitation and martensitic transformation initial and final temperatures, a dilatometric test was performed. The tests were performed on a Netzsch DIL 402-C dilatometer, using a gas flow system composed of 95% argon and 5% hydrogen. The sample used in this test was machined in cylindrical samples, with 6 mm in diameter and 10 mm length. The cycle applied, consisted of heating up to 1030°C at a 10°C / min rate, remaining at this temperature during 0.5 h, and cooling from 20°C / min to room temperature.

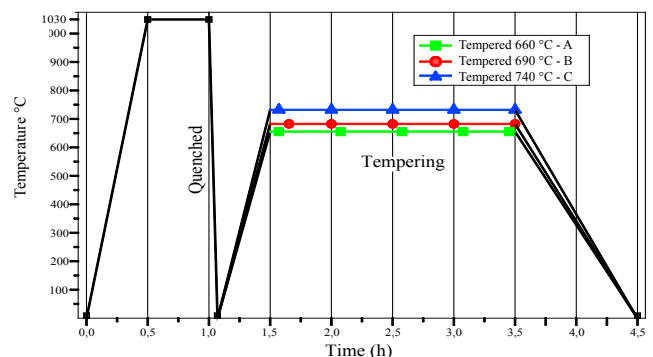## 2.2. Heat Treatment

Figure 3.   Schematic representation of the parameters used in the heat treatment of the samples

The heat treatments used in the samples consisted of austenitization at 1030°C during 0.5 h, quenching in oil (ISO VG 46) and tempering at temperatures of 660°C (cycle A), 690°C (cycle B) and 740°C (cycle C) during 2.0 h, as shown in Fig. 3. All treatments were performed in a Jung 3012 furnace, with a temperature variation of ± 1°C.

2.3. Hardness and Tensile Test

Vickers hardness tests (HV2) were performed in a Shimadzu HMV-2 microdurometer according to ISO 14577-1 [13], a load of 20 N was applied during 10s. In all samples tested, 10 measurements were performed in random regions, and the average and standard deviations were calculated. The Rockwell C hardness (HRC) of the samples tested after heat treatment was determined in a Mitutoyo Model DUROTWIN - DT 20, C benchtop durometer with a diamond cone, preload of 98.7 N (10 kg) and load of 1471N (150 kg) with a total of five indentations in each sample.

Tensile tests with room temperature extensometry were performed on an Instron 300LX-J3 universal mechanical test machine using a 300 kN load cell. The following mechanical properties were determined: yield tensile (MPa), ultimate tensile (MPa) and total elongation were determined by ASTM E8 / E8M-13 [14].

Two samples were tested for each heat treatment condition, obtaining average and standard deviations. Measurements were adopted proportionally to the standard of samples, with a useful length of 75 mm, 12.5 mm internal diameter and head with M18 screw.

2.4. Microstructural Analysis

The microstructure of the samples was analyzed using optical microscopy (MO), scanning electron microscopy (SEM) and transmission electron microscopy (TEM).

To reveal the microstructure which was to be observed by optical microscopy, a conventional metallographic preparation was carried out by sanding with 1200 grit sandpaper, followed by polishing with alumina of 0.3 µm granulometry. The Bain-Villela reagent, composed of 5 ml of hydrochloric acid, 1 g of picric acid and 100 ml of methanol, was immersed for 150 seconds. The observation of the microstructures was performed on an Olympus BX60M optical microscope, with images obtained through the Leica EC3 camera and processed by the LAZ EZ 2.0 software.

In addition to the characterization performed by optical microscopy and to better observe the morphology of martensite and identification of other possible phases, the samples were analyzed by SEM in a JEOL JSM-6390LV microscope using 15 kV.

A JEOL JEM-1011, with a 100 kV voltage, was applied in the analysis of transmission electron microscopy for the characterization of fine precipitates, dislocations and other microconstituents. The preparation consisted in the cutting of samples with a thickness of approximately 1 mm, followed by sanding to the thickness of 200 µm.

A new cut was made in circles of 3 mm in diameter using a circular punch, with new sanding until the thickness of 70 to 80 µm. Then an electrolytic etch was carried out with a solution of 950 ml of acetic acid and 50 ml of perchloric acid in a Struers TenuPol 5 equipment. The voltage parameters of 17 V, flow 13 and temperature of the etch solution of 10°C. The time of etch ranged from 60 to 90 seconds, until a hole was obtained in central region of the sample.

After preparation, the samples were analyzed in light field, dark field and electron diffraction. The precipitates observed in samples tempered at 690°C were determined using ImageJ 1.48 software.

2.5. Creep Test

Creep tests were performed on STM machines, model MF-1000, with constant load of: 160 and 175 MPa at 600°C. The samples' elongation measurement was done by means of LVDT sensors associated to a Fluke Data Logger. Elongation measurements versus time were performed at 5-minute intervals. The creep tests were performed according to ASTM E-139 [15].

3. Results and Discussion

3.1. Characterization of Material

Table 1 presents the chemical composition of the steel used in this work. Comparing with the range of composition of the standard, it was observed that the material in question met the specification of standard EN10269 DIN X22CrMoV12-1 [9].

Table 1. Chemical composition (weight %) of X22CrMoV12-1 steel examined. Reference values according to EN10269

Content	Content of elements in weight - %								
	C	Mn	P	S	Si	Ni	Cr	Mo	V
Value	**0,22**	**0,53**	**0,006**	**0,002**	**0,29**	**0,69**	**11,06**	**0,91**	**0,26**
Max. Norm	0,24	0,90	0,025	0,015	0,50	0,80	12,50	1,20	0,35
Min. Norm	0,18	0,40	-	-	-	0,30	11,00	0,80	0,25

Through the analysis of the dilatometry presented, the inflection of the curve that characterizes the beginning (Pi) and end (Pf) of the precipitation in the steel X22CrMoV12-1, between 761 and 791°C was identified. The start (AC1) of the austenite formation occurred at 846°C and its end (AC3) at 891°C. On cooling, expansion inflection indicated the start (Mi) of the martensite formation at 278°C with its end (Mf) at 121°C - Fig. 4.

Fig. 4 show the initial and final temperature (Pi and Pf) and start and finish of the martensite formation (Mi and Mf). The red line shows the linear expansion and the blue line the corresponding temperature.
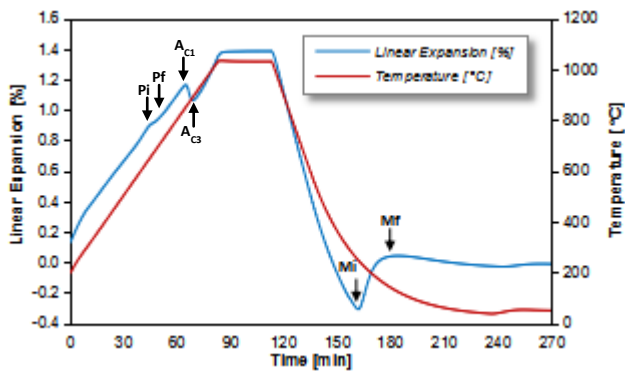
Figure 4.   Dilatometric curve of the X22CrMoV12-1 steel

3.2. Microstructural Analysis

The microstructure of the tempered sample consists of slatted martensite, Fig. 5 (a), with high density of dislocations, Fig. 5 (b), due to the shear distortions imposed on the lattice by the martensitic transformation. No precipitates were observed in this sample.
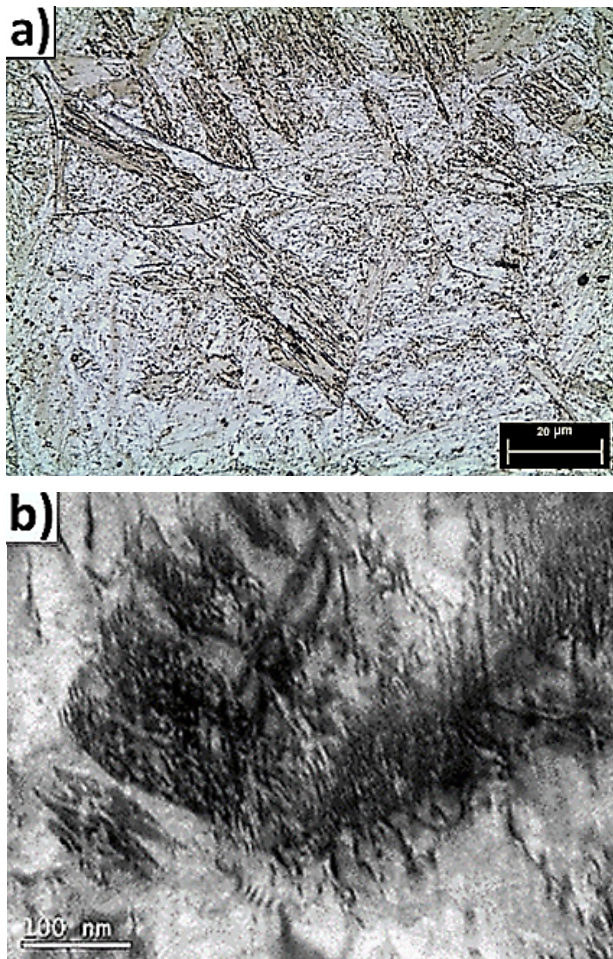

Figure 5.   (a) Martensitic microstructure of tempered X22CrMoV12-1 steel, optical microscopy. Etching, Bain-Vilella. (b) bright field, TEM, sample after quench, showing high density of dislocation in untempered martensite
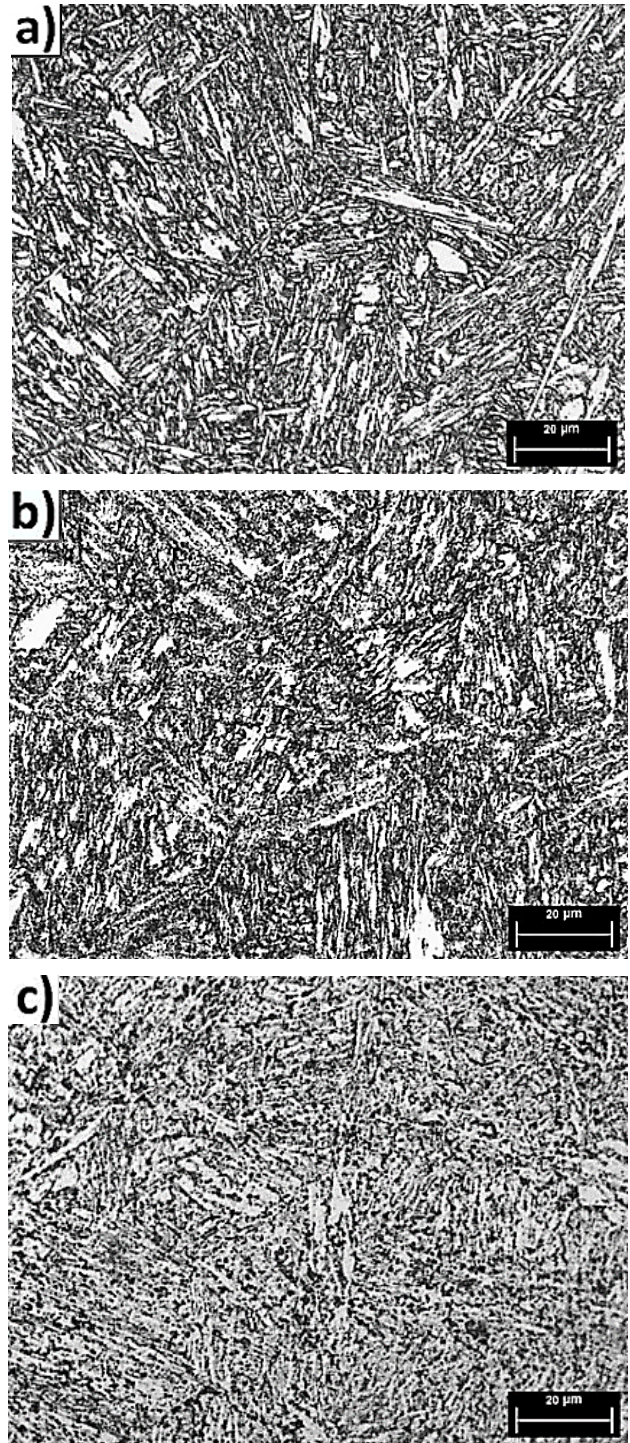

Figure 6.   Microstructures of X22CrMoV12-1 steel quenched and tempered at 660 (a), 690 (b) and 740°C (c) obtained by optical microscopy, consisting of annealed martensite. Etch Bain-Vilella

The optical microscopy and scanning electron microscopy of quenched and tempered X22CrMoV12-1 steel presented a microstructure consisting of annealed martensite. The samples tempered at 660 and 690°C - Figures 6 and 7 - showed martensite slats with similar morphology and well-defined blocks. The tempered samples at 740°C shown in Fig. 6 (c) and 7 (c), showed

partially coalesced slats. By scanning electron microscopy, it was also observed the formation of nucleated precipitates mainly in the contours of the slats, Fig. 7. According to Yan *et al.* [19] coalescing and precipitation are attributed to acceleration of carbon diffusion due to the high temperatures used.
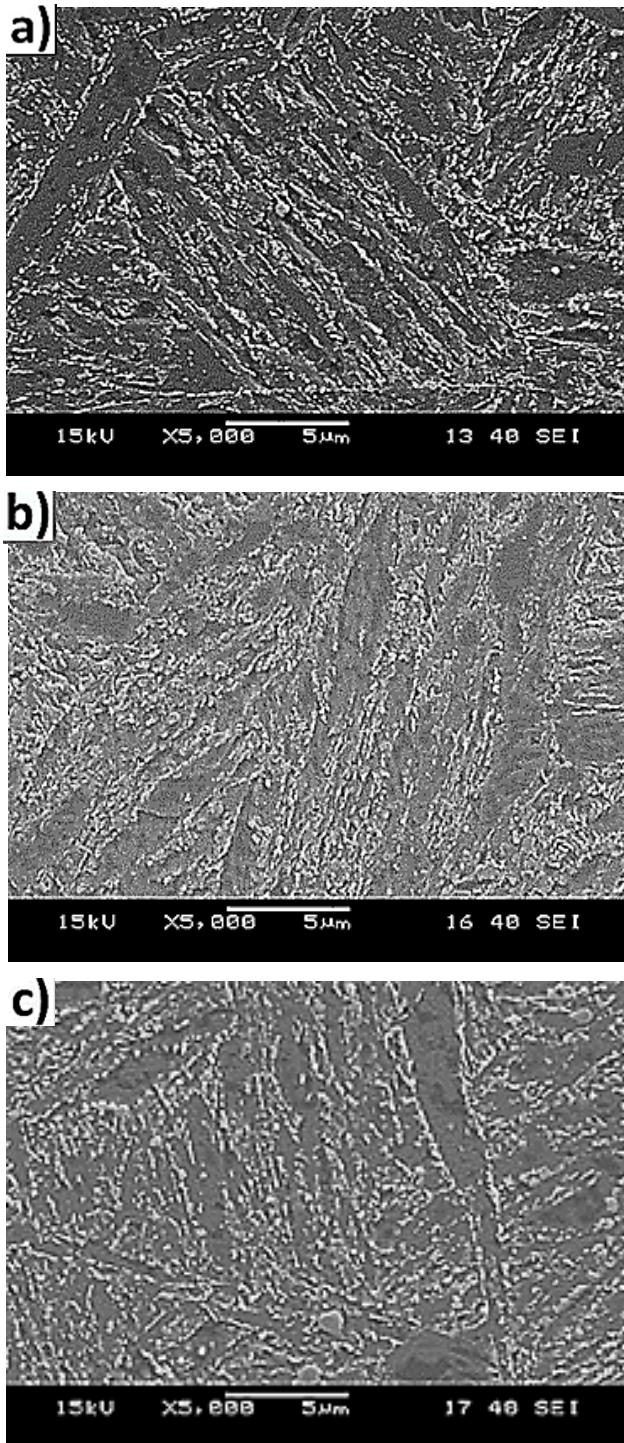

Figure 7. Microstructures of X22CrMoV12-1 steel quenched and tempered at 660°C (a), 690°C (b) and 740°C (c) obtained by scanning electron microscopy
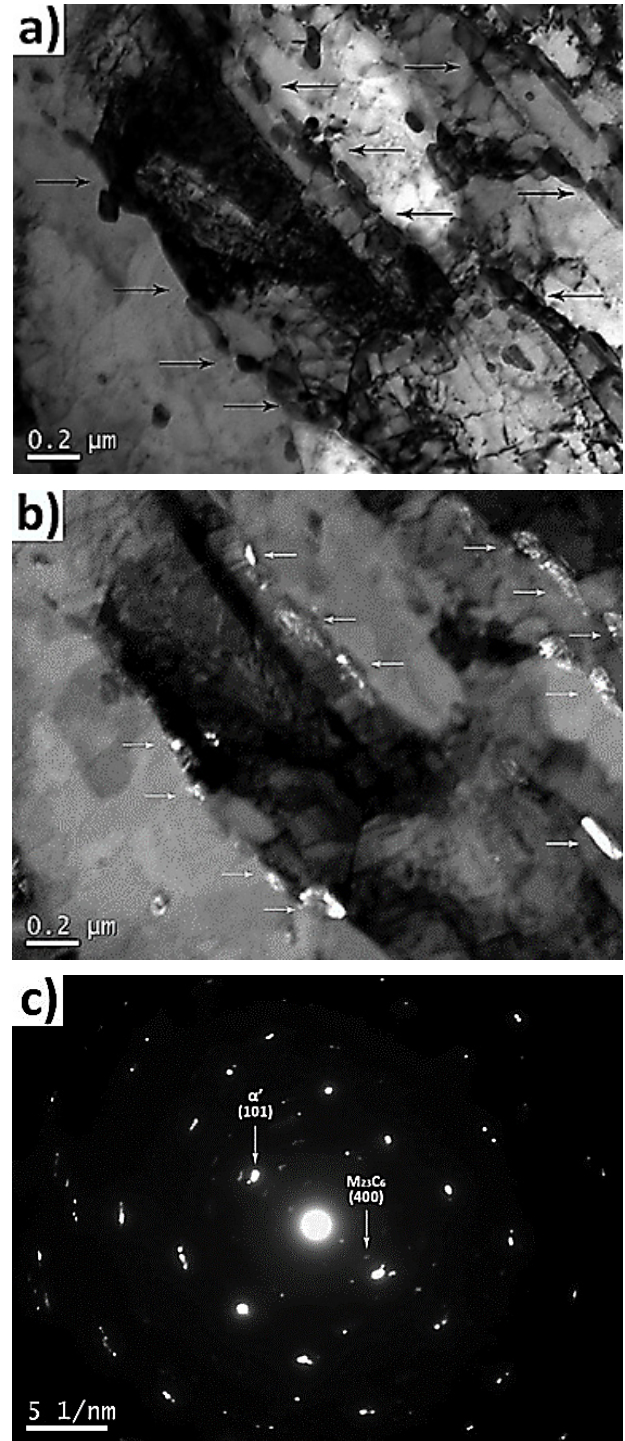

Figure 8. Microstructures (TEM) of steel tempered at 690°C

In the analysis by transmission electron microscopy, all the tempered conditions presented precipitated $M_{23}C_6$ carbides in the contours of the martensite slats. In the sample at 690°C the $M_{23}C_6$ carbide precipitation was observed both in the contours of martensite slats and in the contours of the blocks and packages, and inside, but in smaller amounts – Fig. 8 (a) and (b). These carbides preferably form in contours due to the lower energy barrier for their nucleation. $M_{23}C_6$ carbides had an average length

of 172 ± 27 nm and a width of 66 ± 13 nm. The analysis of the diffraction pattern, Fig. 8 (c), showed, besides the $M_{23}C_6$ carbide, the diffraction of the martensitic matrix. Precipitation of the $M_{23}C_6$ carbide in the contours of blocks, packages and slats in tempered X22CrMoV12-1 steel was also observed by Panait *et al*. [21] and Yan *et al*. [19].

Precipitates with an average diameter of 5 ± 1 nm were also observed inside the slats (Fig. 9) along discordances. The diffraction pattern for these carbides was not obtained, but according to the size, morphology and composition of the steel, can be characterized as MX carbonitrides. These carbonitrides were also identified by Zheng-Fei (2003), Panait *et al* (2010), Fournier *et al* (2011) and Shrestha (2013), with the same observed morphological characteristics.

Fig. 8 (a) show bright field indicating carbides on the border of martensite slats black arrows and Fig. 8 (b) show dark field evidencing the presence of $M_{23}C_6$ white arrow carbides; (c) martensite electron diffraction (α ') indicating reflections (101) and $M_{23}C_6$ (400) precipitates.
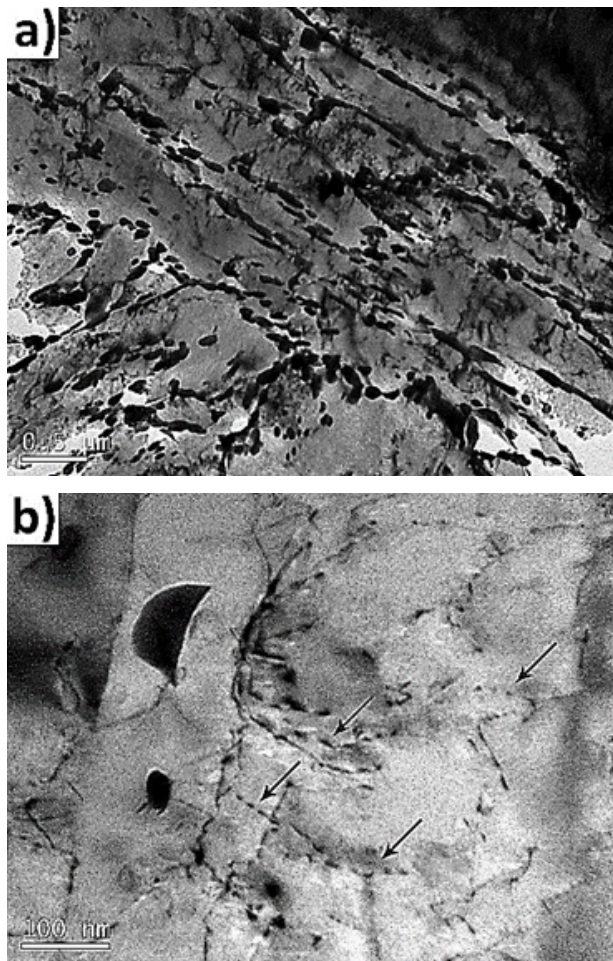

Figure 9. MET bright fields from samples tempered at 690°C: (a) $M_{23}C_6$ carbides along the border of martensite slats; (b) probable MX carbides in dislocations inside slats, indicated by arrows

3.3. Results of Hardness and Tensile Test

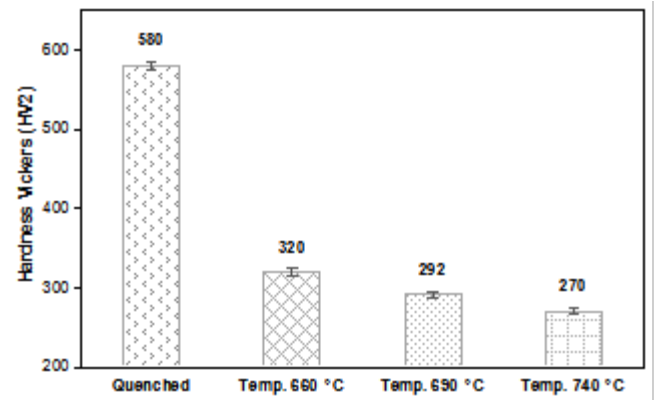The Vickers hardness (HV2) of the heat-treated samples are shown in Fig. 10.

Figure 10. Results of hardness Vickers (HV2) of the samples tempered at 660, 690 and 740°C

The hardness in the only tempered sample was 580 HV - 54 HRC. These results revealed that the higher hardness after tempering heat treatment was obtained with the temperature of tempering at 660°C (320 HV - 32 HRC). The hardness fell approximately linearly by employing the tempering temperatures of 690°C (291 HV - 28 HRC) and 740°C (270 HV - 26 HRC). This reduction is caused by the precipitation of carbides, and the recovery and recrystallization of the martensitic structure. The hardness reductions were expected due to the microstructural modifications that occur in the tempering. Increasing the tempering temperature tends to progressively reduce hardness, strength and flow limits and increase elongation [16, 17].

The results of the tensile tests are presented in Table 2, in which the same hardness behavior was found, that is, the yield and strength limits showed reduction with the increase of the tempering temperature. At 690°C the sample had a reduction of its yield limit of 17% when compared to the tempering at 660°C. The samples tempered at 740°C presented approximate decreases of 14% and 19% in the yield and strength limit values, respectively, in relation to the material tempered at 660°C.

This resistance reduction can be attributed to the greater microstructural transformation of the martensite, higher tempering temperatures aim to return to the material its ductility after the tempering treatment and, consequently reduce its hardness, which is reflected in the reduction of its resistance. The total elongation of the samples increased with the elevation of the tempering temperature, providing greater ductility to the material [18].

Table 2.   Results of tensile test of the tempered samples

Tempered (°C)	Yield Tensile Strength (MPa)	Ultimate Tensile Strength (MPa)	Elongation at Break (%)
660 °C	$\bar{\bar{X}}$=780.0 ± 24.0	$\bar{\bar{X}}$=946.0 ± 0.0	$\bar{\bar{X}}$=18.0 ± 2.0
690 °C	$\bar{\bar{X}}$=649.0 ± 5.7	$\bar{\bar{X}}$=824.5 ± 3.5	$\bar{\bar{X}}$=23.5 ± 2.0
740 °C	$\bar{\bar{X}}$=632.0 ± 0.0	$\bar{\bar{X}}$=810.5 ± 3.5	$\bar{\bar{X}}$=25.0 ± 2.0

3.4. Creep Test

The creep tests result of tempered steels at 660, 690 and 740°C are reported in Tables 3 and 4, showing the results of the minimum creep rate, creep strain and rupture time. The rupture time and the minimum creep rate were shown to be load dependent. The increase of only 15 MPa was enough to reduce the rupture time and the minimum creep rate by significantly modifying the creep curves – Fig. 11 and 12.

Table 3. Results of creep tests for tempered steels – Strain 160 MPa and Test Temperature 600°C

Tempered	Creep Strain (%)	Minimum Creep Rate (%/h)	Rupture Time (hours)
660 °C	8.2	0.0004004	2000
690 °C	7.4	0.0002056	2497
740 °C	15.9	0.0006358	1343

Table 4. Results of creep tests for tempered steels – Strain 175 MPa and Test Temperature 600°C

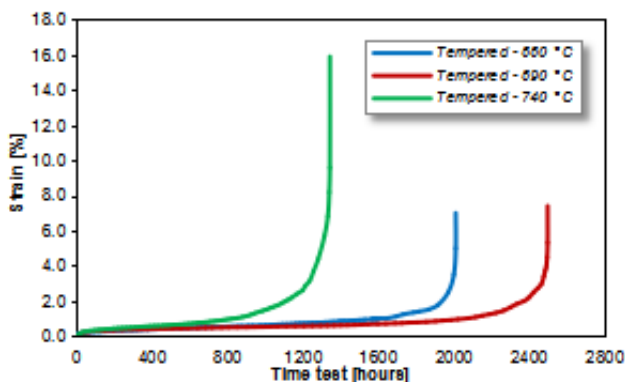| Tempered	Creep Strain (%)	Minimum Creep Rate (%/h)	Rupture Time (hours)
660 °C	7.8	0.0006616	1262
690 °C	6.5	0.0004308	1468
740 °C	16.8	0.0066179	421

Figure 11. Creep curves for steels tempered at 660, 690 and 740°C - Tensile strength 160 MPa and test temperature 600°C
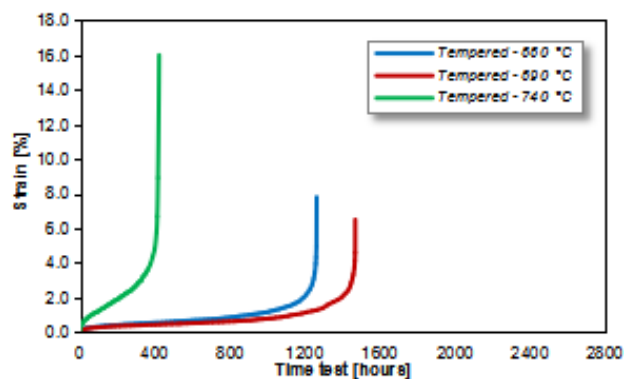

Figure 12. Creep curves for steels tempered at 660, 690 and 740°C - Tensile strength 175 MPa and test temperature 600°C

According to the results, it was observed that the variation of the test load reduced the rupture time by 37% of sample tempered at 660°C, 41% in the 690°C, and 68% in the 740°C sample.

Through the lower slope of the curves during the test it is possible to verify that the X22CrMoV12-1 steel tempered at 690°C has a lower minimum creep rate when compared to the other conditions tested. It was also observed that this condition was the one where the longest times until fracture (2497 and 1468 hours, respectively) was obtained, which is a good indication of its resistance to creep fracture.

4. Conclusions

Analyses of the conditions of tempering studied by optical and scanning electron microscopy did not show clear modifications microstructures between them. In the 740°C condition, slight spheroidization of the martensite slats was observed in relation to the other tempering temperatures.

In the analysis by transmission electron microscopy, all the tempered conditions presented microstructure with $M_{23}C_6$ carbides located in the contours of the martensite slats. Steel tempered at 690°C revealed the presence of $M_{23}C_6$ precipitates with an average length of 172 ± 27 nm and a width of 66 ± 13 nm. Precipitates with an average diameter of 5 ± 1 nm were also observed inside the martensite slats. The diffraction pattern for these carbides was not obtained, but according to the size, morphology and composition of the steel, they can be characterized as MX carbonitrides.

The results of the hardness measurement and the mechanical properties determined in the cold tensile tests showed that the increase of tempering temperature influences the mechanical strength of the studied steel. Higher tempering temperatures promoted the lowering of mechanical properties with increased elongation.

In the creep tests values of rupture time and minimum creep rate were found to be dependent on the test voltage, the increase of only 15 MPa was enough to reduce the values significantly. The X22CrMoV12-1 steel tempered at 690°C showed superior performance on creep resistance between the tempered temperatures tested. In this condition were obtained, respectively, lower creep rates and longer times until there were ruptured, among the samples studied.

All the samples submitted to the creep rupture test presented the three stages: primary, secondary and tertiary, fact proven by their curves. No creep voids were detected among the samples tested, since according to literature, tests with a time greater than 10.000 hours are required for these to be detected.

ACKNOWLEDGEMENTS

REFERENCES

[1] Reed, R. C. "The Superalloys: Fundamentals and Applications". Cambridge University Press, 2006.

[2] Turazi, A. "Estudo da Evolução Microestrutural de Superligas a Base de Níquel Durante Envelhecimento e Tratamentos de Rejuvenescimento de Pás de Turbina a Gás". Tese de Doutorado: PGMAT/UFSC, Florianópolis, 2014.

[3] ASM – American Society For Metals. "Corrosion". Metals Handbook Vol. 13. Ohio: Metals Park, 2004.

[4] Abe, F.; Kern, T.; Viswanathan, R. "Creep-Resistance Steels. CRC, 2008.

[5] Viswanathan, R. "Damage Mechanisms and Life Assessment of High-Temperature Components". USA: ASM International, 1995.

[6] Singh, M. P.; Lucas, G. M. "Blade Design and Analysis for Steam Turbines". McGraw-Hill, p. 364, 2011.

[7] Santos, D.; Cabrita, I.; Gulyurtlu, I. "Materiais Para Caldeira e Turbinas de Centrais Termoelétricas Avançadas". Ciência & Tecnologia dos Materiais, Vol. 23. Lisboa, 2011.

[8] Gandy, D. "X20CrMoV12-1 Steel Handbook". USA: Electric Power Research Institute, 2006.

[9] European Standards – EN 10269 (2014-2). "Steels and Nickel Alloys for Fasteners with Specified Elevated and/or Low Temperature Properties". Germany, 2014.

[10] Ennis, P.; Czyrska-Filemonowicz, A. "Recent Advances in Creep-Resistant Steels for Power Plant Applications", 2003.

[11] Oliveira, A. R. "Determinação de Vida Residual Através de Análise Metalográfica em Tubos de A-312 TP 304H Sujeitos ao Mecanismo de Fluência". Dissertação de Mestrado: UFSC/POSMEC, Florianópolis, 2006.

[12] Meyers, M; Chawla, K. "Mechanical Behavior of Materials". Second Edition. Cambridge – University Press, 2009.

[13] ISO 14577-1 Metallic Materials Instrumental Indentation Test For Hardness and Materials Parameter – Part 1, 2002.

[14] ASTM E8/E8M-13 Standard Test Methods for Tension Testing of Metallic Materials.

[15] ASTM E139-11 Standard Test Methods for Conducting Creep, Creep-Rupture, and Stress-Rupture Tests of Metallic Materials.

[16] Yan, W.; Wang, W.; Sha, Y.Y.; YANG, K. "Microstructural Stability of 9–12%Cr Ferrite/Martensite Heat-Resistant Steels". Frontiers of Materials Science, 2013.

[17] Morito, S.; Adachi, Y.; Ohba, T. "Morphology and Crystallography of Sub-Blocks in Ultra-Low Carbon Lath Martensite Steel". Materials Transactions, v. 50, n. 8, p. 1919–1923, 2009.

[18] Zheng-Fei, H.; Zhen-Guo, T. "Identification of the Precipitates by TEM and EDS in X20CrMoV12. 1 After Long-Term Service at Elevated Temperature". Journal of Materials Engineering and Performance, 2003.

[19] Panait, C.; Zielinska-Lipiec, A.; Koziel, T.; Czyrska-Filemonowicz, A.; Gourgues-Lorenzon, A.F.; Bendick, W. "Evolution of dislocation density, size of subgrains and MX-type precipitates in a P91 steel during creep and during thermal ageing at 600C for more than 100.000 h, 2010".

[20] Fournier, B.; Dalle, F.; Sauzay, M. "Comparison of Various 9–12% Cr Steels Under Fatigue and Creep-Fatigue Loadings at High Temperature". Materials Science & Engineering A, 2011.

[21] Shrestha, T.; Potirniche, G.P.; Basirat, M.; Charit, I. "Creep Rupture Behavior of Grade 91 Steel". Materials Science & Engineering A, 2013.

[22] Lemos, G. "Efeito da Temperatura de Revenido na Microestrutura e nas Propriedades Mecânicas em Alta Temperatura do Aço X22CrMoV12-1". Dissertação de Mestrado: UFSC/PGMAT, Florianopolis, 2006.

[23] Thomson, R.; Bhadeshia, H. "Carbide Precipitation in 12Cr1MoV Power Plant Steel". Metallurgical Transactions, 1992.